

**SYNTHESIS, STRUCTURE AND MAGNETIC PROPERTIES OF DISTORTED  
Y<sub>x</sub>La<sub>1-x</sub>FeO<sub>3</sub>: EFFECTS OF MECHANOCHEMICAL ACTIVATION AND  
COMPOSITION**

A.A Cristóbal <sup>1</sup>, P.M. Botta <sup>1</sup>, E.F. Aglietti <sup>2</sup>, M.S. Conconi <sup>2</sup>, P.G. Bercoff <sup>3</sup>  
and J.M. Porto López <sup>1</sup>

<sup>1</sup> Instituto de Investigaciones en Ciencia y Tecnología de Materiales, INTEMA (CONICET-UNMdP), J.B. Justo 4302 (B7608FDQ) Mar del Plata, Argentina.

<sup>2</sup> Centro de Tecnología de Recursos Minerales y Cerámica, CETMIC (CIC-CONICET), Camino P. Centenario y 506 (B1897ZCA) Gonnet, Argentina.

<sup>3</sup> Facultad de Matemática, Astronomía y Física, FaMAF (UNC) and IFEG (CONICET), Ciudad Universitaria (5000) Córdoba, Argentina.

## **Abstract**

The influence of the mechanochemical treatment on the synthesis and properties of  $Y_xLa_{1-x}FeO_3$  ( $0 \leq x \leq 1$ ) orthoferrites is studied. Solid mixtures of the corresponding metal oxides were treated in a high-energy ball-mill. X-ray diffraction revealed that during the milling the disappearance of the reactants and a fast conversion to orthoferrite phase take place. Magnetic measurements showed a weak ferromagnetic behavior of the obtained materials, observing higher magnetization for larger  $x$ . The activated powders heated at 600 and 800°C showed a progressive crystalline ordering together with a significant drop of magnetization. Thermal treatments at 1000°C produced the formation of the phase  $Y_3Fe_5O_{12}$  for the samples richer in yttrium, increasing the magnetization. Rietveld refinements of the diffraction patterns and dynamical scanning calorimetry were used respectively to determine the lattice parameters and Néel temperatures for the formed orthoferrites. The effect of the composition on the structure and magnetic behavior is discussed.

**Keywords:** mechanochemistry, orthoferrite, magnetic properties

## 1. INTRODUCTION

Perovskites with general formula  $ABO_3$  constitute one of the more extensively studied families of inorganic compounds. This is due to the plethora of functional properties that can be achieved by the modification of its structure through the incorporation of different cations [1,2]. When position B is occupied by Fe, the term orthoferrite is often used to refer to this series of compounds. Depending on the size of cation A, orthoferrites can adopt ideal perovskite structures (cubic) or distorted ones (tetragonal, rhombohedral). The distortion is produced by the cooperative tilting of the  $FeO_6$  octahedra around their own axes [3]. All the combinations of possible tilts give rise to a variety of space groups. The most critical requirement for the formation of a perovskite structure is the ability of cation B to support an octahedral coordination and cation A to support a dodecahedral one. This establishes limits for the radii of both ions, which are commonly expressed by the tolerance factor of Goldschmidt,  $t$  [4] :

$$t = (r_A + r_O) / \sqrt{2} \cdot (r_B + r_O),$$

where  $r_A$ ,  $r_B$  and  $r_O$  are the ionic radii of cation A, cation B and oxygen anion, respectively.

The cubic ideal structure has a value of  $t=1$ , but perovskite structure exists in the range  $0.75 < t < 1$ .

In the case of  $LaFeO_3$ , although the crystal symmetry is orthorhombic, two lattice parameters are almost identical while the third one is clearly larger, giving rise to a quasi-tetragonal structure [5]. In the past decade pure or doped  $LaFeO_3$  has been subject of numerous studies, because of its potential applications in environmental catalysts [6,7], solid oxide fuel cells [8,9], sensors [10] and permeation membranes [11]. From the magnetic point of view, the orthoferrite structure can be described as a two-sublattice system formed by  $FeO_6$  octahedra strongly antiferromagnetically coupled and slightly canted, producing a net magnetic moment

perpendicular to the antiferromagnetic axis. The canting angle is of the order of milliradians and depends on the A-cation size [12]. These features and the extraordinary domain-wall motion of these compounds make them applicable in magneto-optical devices, such as switches and sensors [13-14].

$\text{YFeO}_3$ , presents also an orthorhombic structure, with lattice parameters that differentiate among them much more than in the case of  $\text{LaFeO}_3$ . In this way, the incorporation of a smaller cation, such as Y, to the  $\text{LaFeO}_3$  structure decreases the tolerance factor, presumably leading to reduce the crystal symmetry.

Conventional solid-state reaction method has been used for the synthesis of  $\text{LaFeO}_3$ . This involves grinding and subsequent thermal treatment at 1300-1500°C of the parent oxides [15,16]. Although the method is quite simple and produces single phase  $\text{LaFeO}_3$ , there are some drawbacks such as slow kinetics and uncontrolled particle size and specific surface. For  $\text{YFeO}_3$  the situation is more complicated because of the formation of secondary phases  $\text{Fe}_3\text{O}_4$  and  $\text{Y}_3\text{Fe}_5\text{O}_{12}$  (YIG) [17]. Alternative synthetic routes have been developed, such as co-precipitation, combustion, sol-gel, etc. [18-20]. In these wet chemical methods, pure phase formation can be accelerated and also the particle size and morphology can be much more controlled.

In the last years, a couple of studies about the synthesis of  $\text{LaFeO}_3$  by mechanochemical activation of oxide precursors have been reported [21,22]. This powder-processing technique consists in a high energy ball-milling of solid reactants that usually accelerates diffusive processes favoring the completion of solid-state reactions under ambient conditions. Frequently, the compounds obtained in this way have a metastable structure that confers them special properties. For this reason this method has been applied in the last decades to prepare a variety of materials with electrical and magnetic properties [23-25]. According to Cristóbal et al. [22] mechanosynthesized  $\text{LaFeO}_3$  exhibited a relatively high saturation magnetization,

which is associated to the accumulation of numerous defects in the crystal structure during the mechanical treatment. The replacement of a half of La by Y cations increases the structural distortion and produces a significant rise in the magnetization [26].

On this basis we propose in the present work the modification with yttrium of lanthanum perovskite in the whole range of composition, aiming to determine the combined effect of doping and mechanochemistry on the structure and magnetic properties of these materials.

## **2. EXPERIMENTAL**

### **2.1. Materials**

Starting materials were  $\text{Fe}_3\text{O}_4$  (a magnetite concentrate ore, 97.5 wt%),  $\text{La}_2\text{O}_3$  and  $\text{Y}_2\text{O}_3$  (both commercial reagents, 99.9 wt%). Powder mixtures with different molar ratio were prepared and mechanochemically activated in a Fritsch Pulverisette 7 planetary ball-mill. Cr-hardened steel vials were rotated at about 1500 rpm, each one containing 7 balls and 5 g of powder resulting in a ball-to-powder ratio of 20. Oxygen supply was assured by means of a periodic opening of the vials. Also small amounts of sample were withdrawn in order to study the evolution of the reaction throughout the mechanical treatment. Five compositions with yttrium contents (x in the formula  $\text{Y}_x\text{La}_{1-x}\text{FeO}_3$ ) ranging between 0 and 1 were prepared. The series of samples were named YML-x-yh where x is the Y content and y the activation time in hours.

The activated powders were submitted to thermal treatments between 600 and 1000°C for 30 minutes in air atmosphere.

## 2.2. Characterization techniques

Evolution of the mixtures' composition was followed by XRD using a PW 1830/40 diffractometer at 40 kV and 30 mA, with  $\text{CoK}\alpha$  radiation ( $\lambda = 1.789 \text{ \AA}$ ). Lattice parameters were determined for each composition by means of the Rietveld method. The refinements were made on patterns taken under special conditions: a step size of  $0.02^\circ 2\theta$  with 5 seconds of counting time per step.

For samples with  $x \leq 0.5$  the refinement routines were initiated with crystallographic data of  $\text{LaFeO}_3$  [5], while for samples with  $x > 0.5$  the refinements were made starting from  $\text{YFeO}_3$  structure [27]. In this way lattice parameters and occupancy factors were refined for the whole series of calcined samples.

Magnetization (M) at room temperature as a function of applied field (H) was measured using a Lakeshore 7300 vibrating sample magnetometer. Magnetic loops between +15 and -15 kOe were registered.

Differential scanning calorimetry (DSC) was used to determine Néel temperatures ( $T_N$ ) of the orthoferrite phases present in calcined samples. The scans were performed in a Shimadzu DSC-50 calorimeter, using a heating-cooling rate of  $10^\circ\text{C min}^{-1}$ .

## 3. RESULTS AND DISCUSSION

Figure 1 shows the XRD patterns of the series of activated samples for  $x = 0.25$  (a) and  $0.75$  (b). For both compositions the consumption of reactants is clearly observed after 1 h of milling. Simultaneously, peaks corresponding to orthoferrite phase start to be visible. After 3 h of mechanical treatment the diffraction signals corresponding to the reactants have disappeared and only peaks ascribed to orthoferrite ( $\text{Y}_{0.25}\text{La}_{0.75}\text{FeO}_3$  or  $\text{Y}_{0.75}\text{La}_{0.25}\text{FeO}_3$ ) can be observed. Similar results were obtained for the other compositions.

Figure 2 shows the diffractograms for samples activated for 3 h with  $x$  between 0 and 1. As mentioned above, for the entire composition range all the diffracted peaks belong to the orthoferrite phase. Also, the appearance of additional peaks as Y content increases can be noticed. This is due to the loss of structural symmetry produced by the doping with Y. For  $\text{LaFeO}_3$  the structure is almost tetragonal having one lattice parameter ( $b$ ) larger than the other two ( $a$  and  $c$ ) which are very close each other. By contrast in  $\text{YFeO}_3$  the shorter parameters  $a$  and  $c$  are clearly different between them, leading to the appearance of additional diffraction peaks corresponding to additional crystalline planes. On the other hand, a displacement of the main peaks towards higher angles as Y content increases is observed (see inset of Fig. 2). This is a consequence of the reduction in lattice volume produced by the substitution of La by the smaller Y cation.

From the  $M$  vs  $H$  curves, maximum magnetization (measured at maximum applied field,  $H=15$  kOe) were determined for all the samples. The results are shown in Figure 3, where the variation of  $M_{\text{max}}$  with activation time is presented. The continuous decrease of magnetization is due to the gradual consumption of magnetite, which is a ferrimagnetic oxide with a very high magnetization ( $92 \text{ emu g}^{-1}$  [28]). At the same time, as the reaction progresses the formation of the orthoferrite phases becomes prevalent. Although orthoferrites are essentially antiferromagnetic, their spin magnetic moments are not perfectly ordered in an antiparallel configuration, giving rise to a weak ferromagnetism [12,29]. In summary, the progressive formation of  $\text{Y}_x\text{La}_{1-x}\text{FeO}_3$  (weak ferromagnetic compound) at expenses of  $\text{Fe}_3\text{O}_4$  (ferrimagnetic oxide) leads to a dramatic drop of  $M_{\text{max}}$  after 3 h of mechanical activation.

The inset of Fig. 3 shows the variation of  $M_{\text{max}}$  as a function of yttrium content ( $x$ ) for samples YML- $x$ -1h and YML- $x$ -3h. In both series an increase of  $M_{\text{max}}$  for larger  $x$  values is observed. It is important to remark that as  $x$  grows magnetite content in the starting mixtures increases, according to the stoichiometry of each composition. In samples activated for 1 h

this obviously produces higher magnetization values, since magnetite is a significantly abundant phase in the powder mixture. The same tendency can be noticed for samples activated for 3 h, but in this case the cause for the increment of  $M_{\max}$  can not be the presence of remnant magnetite, according to XRD patterns (see Figs. 1 and 2). As Y replaces La in the perovskite lattice, the structure suffers a distortion produced by the significantly different ionic radii of both cations (1.36 Å for  $\text{La}^{3+}$  and 1.10 Å for  $\text{Y}^{3+}$ ) [30]. This distortion leads to a spin canting which is the responsible for the net magnetic moment measured for each compound.

Figure 4 shows XRD patterns of samples YML-x-3h calcined at 1000°C. The comparison with as-milled powders (Fig. 1) reveals the increase of crystallinity and crystallite size produced by the thermal treatment. The incorporation of yttrium to the perovskite phase is evidenced by the shift to higher angles of the XRD peaks and the appearance of additional signals due to the variation in the lattice parameters (this was also observed for the as-milled series). For  $x \geq 0.5$  small peaks corresponding to a secondary phase can be clearly noticed. These are assigned to YIG, a common impurity in the synthesis of  $\text{YFeO}_3$ , as stated in the Introduction. Weight percentages of this phase were estimated from the refinement of XRD patterns using the Rietveld method. The results (Table 1) show a continuous increase as Y content grows, reaching a maximum value of 15% when  $x=1$ .

Lattice parameters of the orthoferrite phase were refined for all the compositions, and the results are shown in Table 1. These values are presented together with the corresponding lattice parameters of the parent compounds,  $\text{LaFeO}_3$  and  $\text{YFeO}_3$ , which were taken from powder diffraction files database [5,27]. A comparison between the three orthorhombic structures reveals that doping with Y produces a significant decrease of the unit cell volume, which is an expectable effect due to the smaller size of this cation with respect to  $\text{La}^{3+}$ . However, the lattice contraction is not isotropic: parameters  $b$  and  $c$  undergo a pronounced

decrease whereas  $a$  shows a slight increase, indicating a marked distortion of the lattice geometry as the yttrium content grows. Figure 5 summarizes these observations.

Magnetization of samples YML- $x$ -3h-1000 is shown in Figure 6. A gradual increase of  $M_{\max}$  can be noticed up to  $x=0.75$ , which is related to the distortion produced by the growing incorporation of Y in orthoferrite structure. For  $x=1$  a sudden rise is observed due to the presence of an appreciable amount of  $Y_3Fe_5O_{12}$  (see Fig. 4). This is a ferrimagnetic oxide with saturation magnetization about 26-28 emu g<sup>-1</sup> [31,32], which obviously increases the total magnetization. As stated above this garnet is a common secondary-phase in the synthesis of  $YFeO_3$ , so it seems reasonable that its formation was greater for  $x=1$ . The inset shows the variation of  $M_{\max}$  with heating temperature (for as-milled powders we assume 25°C). For the sake of clarity, only curves for  $x=0.25$  and 0.75 are displayed (the rest of compositions exhibits the same tendency). The magnetization continuously diminishes up to 800°C, owing to the gradual elimination of the structural damage generated by the mechanical treatment. However, for samples calcined at 1000°C  $M_{\max}$  increases. At this temperature the formation of YIG becomes more significant, 8 wt.% according to Table 1. For each sample it is possible to estimate the contribution of YIG to the measured magnetization considering the weight percentages obtained by the Rietveld refinement and taking the saturation magnetization for YIG as 27 emu/g. Table 2 summarizes these results, showing a marked similarity between measured magnetizations ( $M_{\text{meas}}$ ) and the calculated ones ( $M_{\text{cal}}$ ). For all the compositions this observation indicates that total measured magnetization is due to YIG, being the contribution of  $Y_xLa_{1-x}FeO_3$  almost negligible. This is reasonable since after heating at 1000°C, most part of the structural disorder accumulated during the mechanical treatment of samples was eliminated, yielding an antiferromagnetically ordered structure for the orthoferrite.

Néel temperatures ( $T_N$ ) of  $Y_xLa_{1-x}FeO_3$  were determined by DSC for each sample YML-x-3h-1000. A continuous decrease of  $T_N$  as  $x$  increases is observed (Fig. 8). The incorporation of Y to the perovskite lattice provokes a destabilization of the magnetic structure, due to the loss of crystal symmetry (see Fig. 5). As a consequence, the thermal energy necessary to break the antiferromagnetic ordering is lower, decreasing the transition temperature.  $T_N$  values obtained from DSC scans are somewhat lower than those reported in literature for the parent compounds [12] (to the best of our knowledge there is not information reported for the other compositions). We obtained  $T_N = 449^\circ\text{C}$  and  $354^\circ\text{C}$  for  $LaFeO_3$  ( $x=0$ ) and  $YFeO_3$  ( $x=1$ ), respectively. By differential thermal analyses, Treves has determined Néel temperatures of  $465$  and  $372^\circ\text{C}$  for these compounds [12]. The lowering of Néel temperature of these materials can be interpreted in terms of a decrease in the number of Fe-O-Fe linkages due to the existence of oxygen and iron vacancies [33]. The presence of lattice defects remaining from mechanochemical treatment in the calcined materials could be the origin of these ionic vacancies.

#### 4. CONCLUSIONS

The mechanochemical activation of  $La_2O_3$ ,  $Y_2O_3$  and  $Fe_3O_4$  in a planetary ball-mill allows synthesizing orthoferrite  $Y_xLa_{1-x}FeO_3$  phases at room temperature in the whole range of composition. The distorted crystal structure produced by 3 h of mechanical treatment and the incorporation of yttrium produces materials with relatively high magnetization. Maximum magnetization of the mechanochemical synthesized orthoferrites increases as yttrium content grows, reaching  $4.20 \text{ emu g}^{-1}$  when  $x=1$ . This is a consequence of the anisotropic distortion underwent by the perovskite structure as Y cations replace La cations, leading to increase the spin canting angle.

Thermal treatments significantly improve the crystallinity and structural ordering, diminishing the magnetization of the materials. At the highest heating temperature (1000°C) the formation of  $Y_3Fe_5O_{12}$  garnet is observed, clearly favored in the compositions richer in Y. XRD Rietveld refinements allowed to determine lattice parameters of orthoferrite phases obtained for each x value after calcinations at 1000°C. The measurement of the Néel temperature shows a gradual decrease with x due to the loss of stability of the magnetic structure caused by the lower symmetry of crystal lattice.

### **ACKNOWLEDGEMENTS**

The authors wish to acknowledge partial funding from CONICET, ANPCyT, UNMdP and SECyT-UNC.

### **REFERENCES**

- [1] J.B. Goodenough, Electronic and ionic transport properties and other physical aspects of perovskites, *Rep. Prog. Phys.* 67 (2004) 1915-1993.
- [2] G. King, P.M. Woodward, *J. Mater. Chem.* 20 (2010) 5785–5796.
- [3] F. Rivadulla, Magnetotransporte y resonancia de spin electrónico en manganitas, Ph.D. thesis, University of Santiago de Compostela, 2000.
- [4] C. Li, K.C. Kwan Soh, P. Wu, *J. Alloys Compd.* 372 (2004) 40–48.
- [5] M. Marezio, P.D. Dernier, *Mater. Res. Bull.* 6 (1971) 23-30.
- [6] P. Ciambelli, S. Cimino, L. Lisi, M. Faticanti, G. Minelli, I. Pettiti, P. Porta, *Appl. Catal. B: Environ.* 33 (2001) 193.
- [7] J. Ding, X. Lü, H. Shu, J. Xie, H. Zhang, *Mater. Sci. Eng. B* 171 (2010) 31–34.
- [8] I. Wærnhus, P.E. Vullum, R. Holmestad, T. Grande, K. Wiik, *Solid State Ionics* 176 (2005) 783 – 790.

- [9] F. Bidrawn, S. Lee, J.M. Vohs, R.J. Gorte, *J. Electrochem. Soc.* 155 (2008) B660-B665.
- [10] N.N. Toan, S. Saukko, V. Lantto, *Physica B* 327 (2003) 279–282.
- [11] Y. Zheng, Y.S. Lin and S.L. Swardz, *J. Membr. Sci.* 150 (1998) 87-89.
- [12] D. Treves, *J. Appl. Physics* 36 (1965) 1033-1039.
- [13] Y.S. Didosyan, H. Hauser, H. Wolfmayer, J. Nicolics, P. Fulmek, *Sens. Actuators A* 106 (2003) 168.
- [14] Y.S. Didosyan, H. Hauser, G.A. Reider, W. Toriser, *J. Appl. Phys.* 75 (2004) 7339-7341.
- [15] J.B. Smith, T. Norby, *Solid State Ionics* 177 (2006) 639–646.
- [16] B. Yan, Q. Feng, J. Liu, K.C. Chou, *High Temp. Mat. Proc.* 28 (2009)101-108.
- [17] D.S. Schmool, N. Keller, M. Guyot, R. Krishnan, M. Tessier, *J. Magn. Mater.* 195 (1999) 291.
- [18] X. Qi, J. Zhou, Z. Yue, Z. Gui, L. Li, *Mater. Chem. Phys.* 78 (2002) 25-29.
- [19] S. Mathur, M. Veith, R. Rapalaviciute, H. Shen, G.F. Goya, W.L. Martins Filho, T.S. Berquo, *Chem. Mater.*16 (2004) 1906-1913.
- [20] P.V. Gosavi, R.B. Biniwale, *Mater. Chem. Phys.* 119 (2010) 324-329.
- [21] Q. Zhang, F. Saito, *J. Mater. Sci.* 36 (2001) 2287-2290.
- [22] A.A. Cristóbal, P.M. Botta, P.G. Bercoff, J.M. Porto López, *Mater. Res. Bull.* 44 (2009) 1036–1040.
- [23] V.V. Boldyrev, *Russ. Chem. Rev.* 75 (2006) 177-189.
- [24] V. Sepelák, U. Steinike, D.C. Uecker, S. Wissmann, D. Becker, *J. Solid State Chem.* 135 (1998) 52–58.
- [25] M. Algueró, J. Ricote, T. Hungría, A. Castro, *Chem. Mater.* 19 (2007) 4982–4990.
- [26] A.A. Cristóbal, P.M. Botta, P.G. Bercoff, E.F. Aglietti, H.R. Bertorello, J.M. Porto López, *J. Alloys Compd.* 495 (2010) 516–519.
- [27] P. Coppens, M. Eibschuetz, *Acta Crystallogr.* 19 (1965) 524- 531.

- [28] J. Smit and H. P. Wijn. Ferrites. Page 157. Philips Technical Library, 1959.
- [29] M. Rajendran, A.K. Bhattacharya, J. Eur. Ceram. Soc. 26 (2006) 3675–367.
- [30] R.D. Shannon, Acta Crystallogr. A 32 (1976) 751.
- [31] P. Vaqueiro, M.A. López-Quintela, J. Rivas, J.M. Greneche, J. Magn. Magn. Mater. 169 (1997) 56–68.
- [32] M.M. Rashad, M.M. Hessian, A. El-Midany, I.A. Ibrahim, J. Magn. Magn. Mater. 321 (2009) 3752–3757.
- [33] H. Yamamura, S. Shirasaki, H. Oshima, K. Kakegawa, J. Solid State Chem. 18 (1976) 329-335.

**Table 1.** Rietveld refinements of XRD patterns of samples YML-x-3h heated at 1000°C. YIG percentages, lattice parameters and volume for  $Y_xLa_{1-x}FeO_3$  phases are also displayed.

x	YIG wt%	Lattice parameters				Refinement parameters			
		a (Å)	b (Å)	c (Å)	V(Å <sup>3</sup> )	R <sub>wp</sub>	R <sub>exp</sub>	R <sub>Bragg</sub>	χ <sup>2</sup>
0	0	5.5447(3)	5.5513(2)	7.8545(4)	241.8	10.6	7.5	2.1	1.99
0.25	< 1	5.4943(2)	5.5563(2)	7.8103(3)	238.4	14.8	7.8	3.5	3.64
0.5	5	5.4152(5)	5.5625(4)	7.7332(3)	232.9	18.0	8.3	7.9	4.70
0.75	8	5.3440(1)	5.5725(1)	7.6648(2)	228.3	11.9	8.3	4.3	2.02
1	15	5.2803(2)	5.5757(1)	7.6001(3)	223.8	9.2	7.4	2.0	1.55
LFO	-----	5.5530(2)	5.5630(2)	7.8670(3)	243.0	-----	-----	-----	-----
YFO	-----	5.2819(2)	5.5957(5)	7.6046(3)	224.8	-----	-----	-----	-----

**Table 2.** Measured and calculated saturation magnetization,  $M_{\text{meas}}$  and  $M_{\text{cal}}$  respectively, for samples YML-x-3h heated at 1000°C.

<b>x</b>	<b><math>M_{\text{meas}}</math> (emu/g)</b>	<b><math>M_{\text{cal}}</math> (emu/g)</b>
0	0.14	0
0.25	0.69	< 0.27
0.5	1.09	1.35
0.75	1.94	2.16
1	4.20	4.05

## Figure captions

**Figure 1.** Diffractograms of the series of activated samples for  $x=0.25$  (a) and  $0.75$  (b). M:  $\text{Fe}_3\text{O}_4$ , Y:  $\text{Y}_2\text{O}_3$ , L:  $\text{La}_2\text{O}_3$ , o:  $\text{Y}_{0.25}\text{La}_{0.75}\text{FeO}_3$ , \*:  $\text{Y}_{0.75}\text{La}_{0.25}\text{FeO}_3$

**Figure 2.** XRD patterns for samples  $\text{YML-x-3h}$ . All the peaks correspond to phase  $\text{Y}_x\text{La}_{1-x}\text{FeO}_3$ . The inset displays an enlargement of the main peak, showing its displacement towards higher angles as the yttrium content increases.

**Figure 3.** Magnetization measured at maximum applied field ( $H=15$  kOe) as a function of activation time for samples  $\text{YML-x}$  ( $0 \leq x \leq 1$ ). The inset shows the variation of  $M_{\text{max}}$  as a function of yttrium content ( $x$ ) activated for 1 h and 3 h.

**Figure 4.** XRD patterns for samples  $\text{YML-x-3h}$  heated at  $1000^\circ\text{C}$ . All the peaks correspond to phase  $\text{Y}_x\text{La}_{1-x}\text{FeO}_3$  except where indicated, G:  $\text{Y}_3\text{Fe}_5\text{O}_{12}$ . The inset displays an enlargement of the central region, showing the displacement of the peaks with the yttrium content.

**Figure 5.** Variation of lattice ( $l$ ) parameters and volume ( $V$ ) as a function of yttrium content for samples  $\text{YML-x-3h}$  heated at  $1000^\circ\text{C}$ .

**Figure 6.** Maximum magnetization ( $M_{\text{max}}$ ) as a function of yttrium content ( $x$ ) for samples  $\text{YML-x-3h}$  heated at  $1000^\circ\text{C}$ . The inset shows the variation of  $M_{\text{max}}$  with heating temperature for samples  $\text{YML0.25}$  and  $\text{YML0.75}$  activated for 3 h.

**Figure 7.** XRD patterns of samples YML-0.25-3h and YML-0.75-3h heated at several temperatures, showing the formation of  $\text{Y}_3\text{Fe}_5\text{O}_{12}$  (G) at 1000°C.

**Figure 8.** Néel temperature as a function of yttrium content (x) for YML-x-3h heated at 1000°C. Inset: DSC curves obtained for YML-0-3h-1000.

Figure(s)  
[Click here to download high resolution image](#)

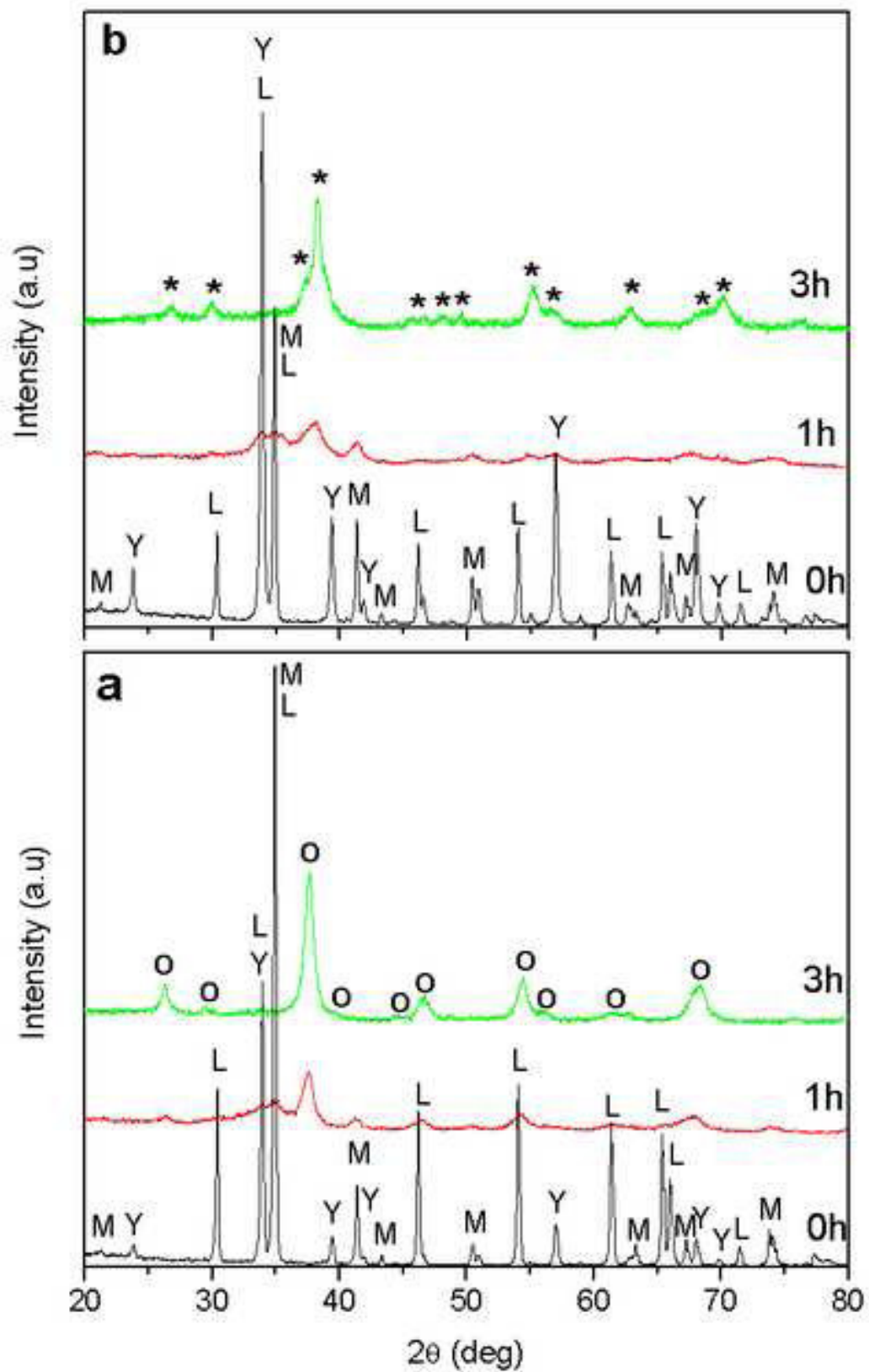


Figure 1

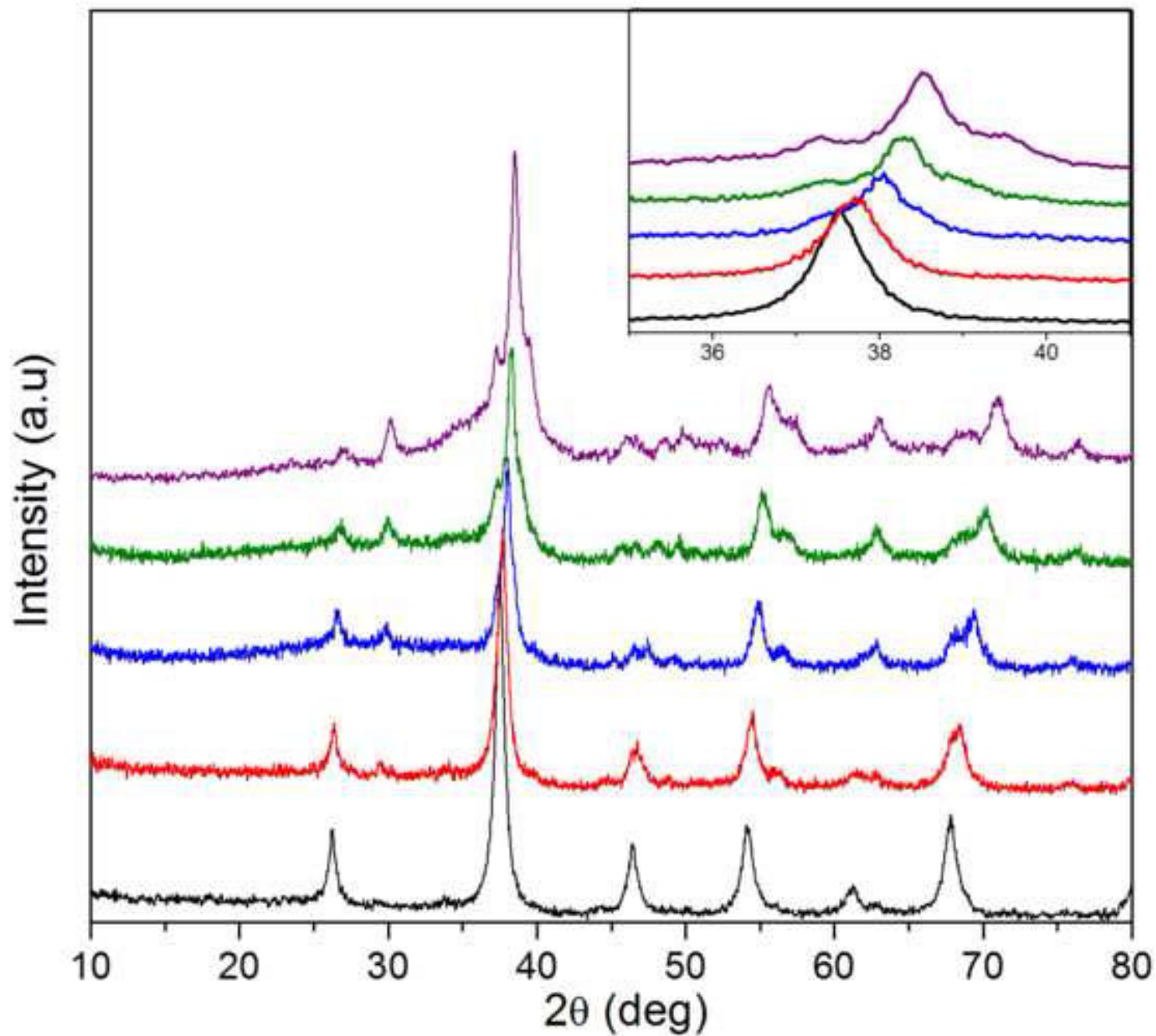


Figure 2

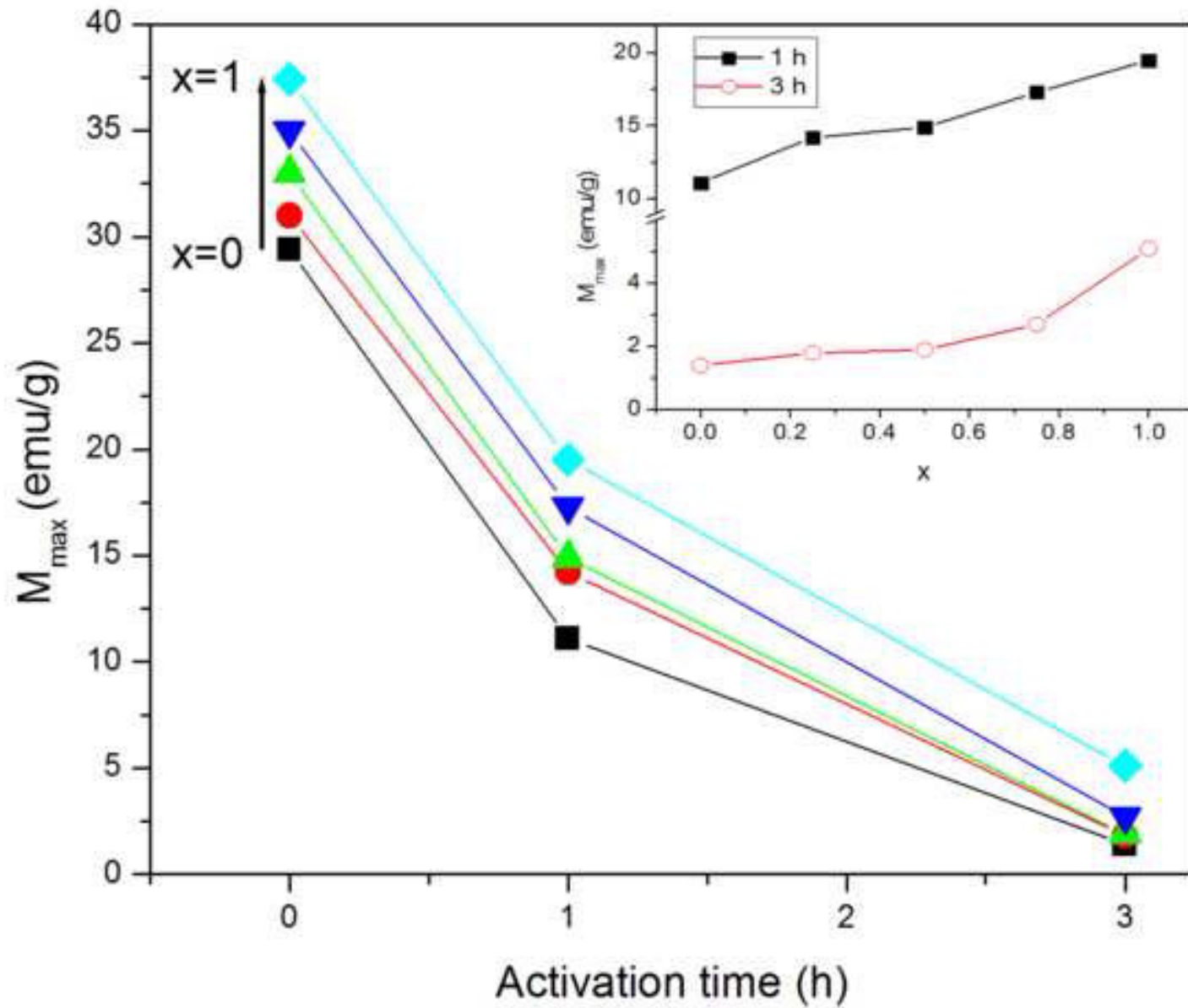


Figure 3

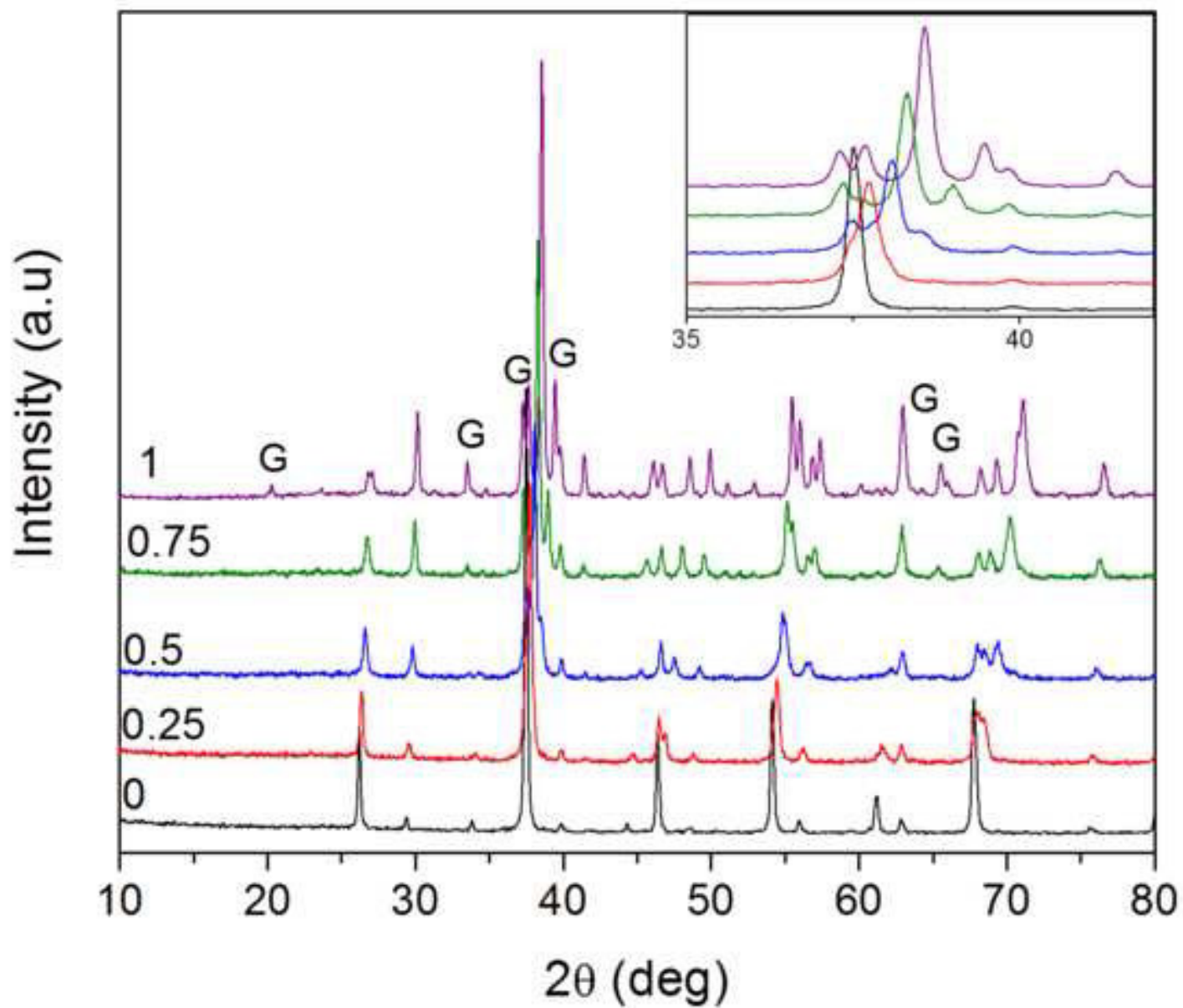


Figure 4

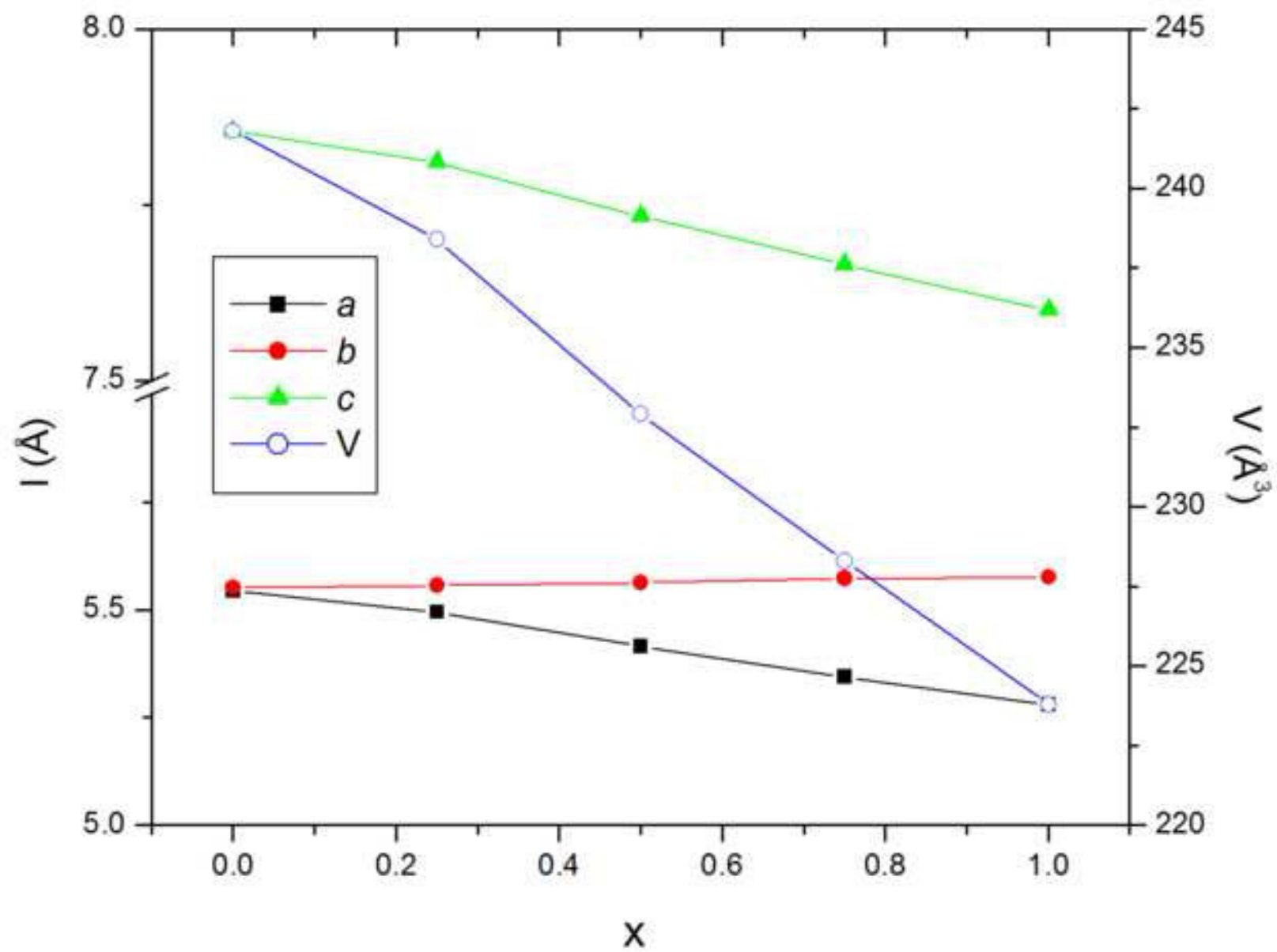


Figure 5

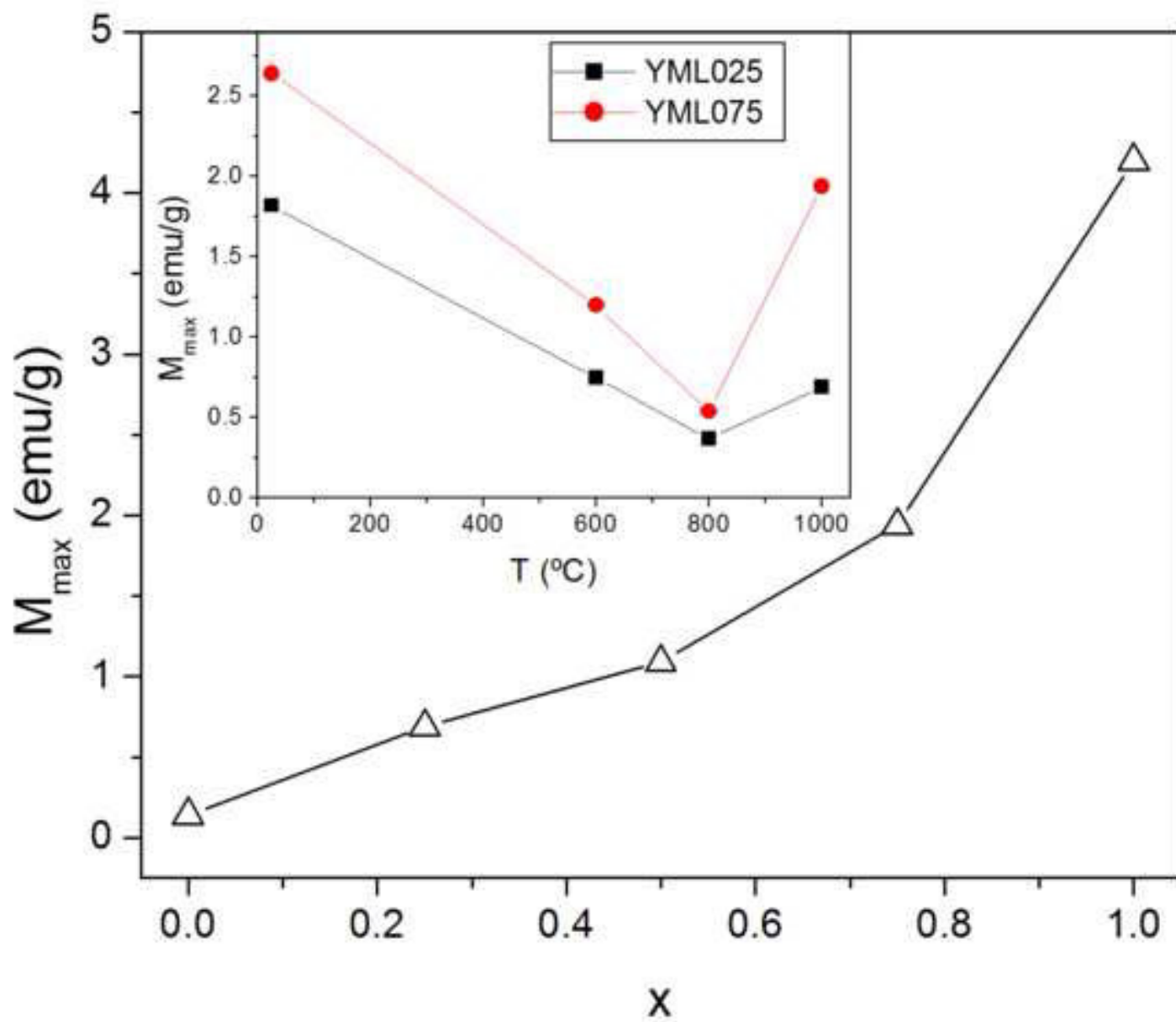


Figure 6

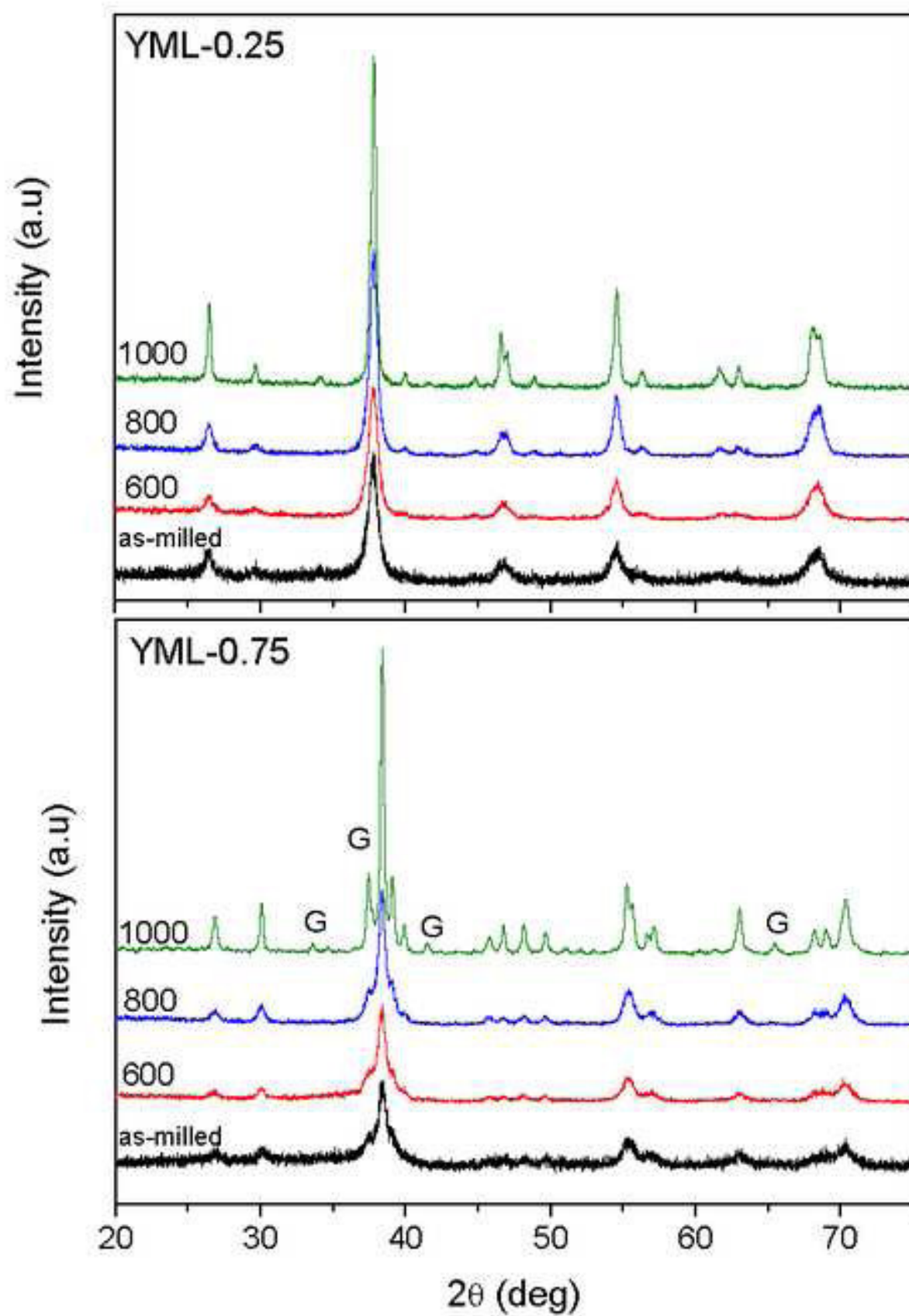


Figure 7

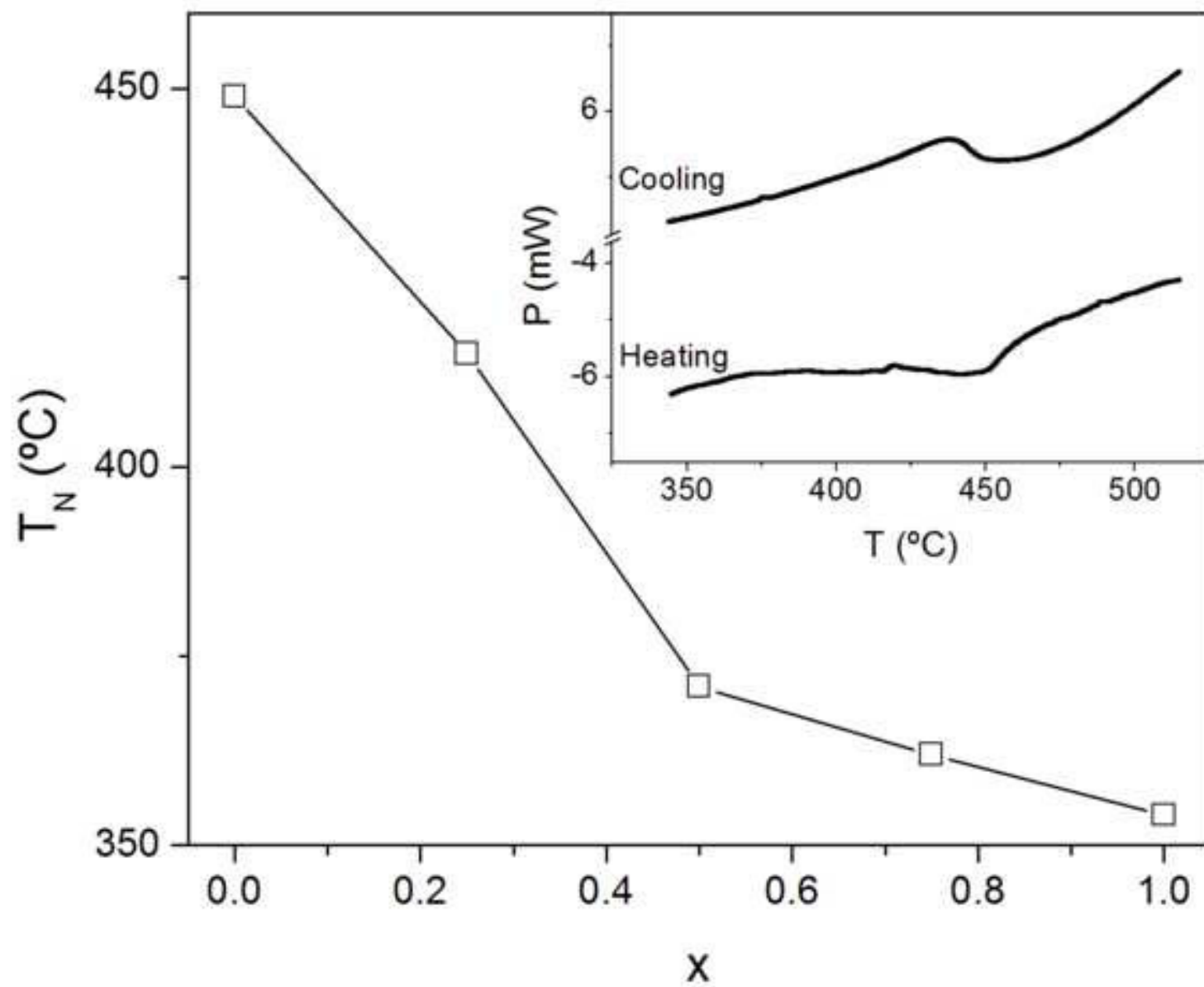


Figure 8